

The Physics Potential of Future Long Baseline Neutrino Oscillation Experiments*

M. Lindner ^a

^aPhysik-Department, Technische Universität München, James-Frank-Strasse, D-85748 Garching, Germany, Email: lindner@ph.tum.de

Different future long baseline neutrino oscillation setups are discussed and the remarkable potential for very precise measurements of mass splittings and mixing angles is shown. Furthermore it will be possible to make precise tests of MSW effects, which allow to determine the sign of Δm^2 . Finally strong limits or measurements of leptonic CP violation will be possible.

1. Introduction

The existing evidence for atmospheric neutrino oscillations includes some sensitivity to the characteristic L/E dependence of oscillations [1], and there is no doubt that the observed flavour transitions are due to neutrino oscillations. Solar neutrinos were also shown to undergo flavour transitions [2,3]. This solves the long standing solar neutrino problem, even though the characteristic L/E dependence of oscillation is in this case not yet established. However, oscillation is under all alternatives by far the most plausible explanation and global oscillation fits clearly favour the so-called LMA solution for the mass splittings and mixings [4,5,6,7]. The CHOOZ reactor experiment [8] provides moreover currently the most stringent upper bound for the sub-leading U_{e3} element of the neutrino mixing matrix. The global pattern of neutrino oscillation parameters seems therefore quite well known and one may ask how precise future experiments will ultimately be able to measure mass splittings and mixings and what can be learned from such precise measurements.

The characteristic length scale L of oscillations is given by $\Delta m^2 L/E_\nu = \pi/2$. The atmospheric Δm_{31}^2 -value leads thus to an oscillation length scale L_{atm} as a function of energy. For $\Delta m_{31}^2 \simeq 3 \cdot 10^{-3} \text{ eV}$, and for neutrino energies of

$E_\nu \simeq 10 \text{ GeV}$, one finds $L_{atm} \simeq \mathcal{O}(2000) \text{ km}$, *i.e.* distances and energies which can be realized by sending neutrino beams from one point on the Earth to another. The solar Δm_{21}^2 is for the favoured LMA solution about two orders of magnitude smaller than the atmospheric Δm_{31}^2 , resulting for the same energies in oscillations at scales $L_{sol} \simeq (10 - 1000) \cdot L_{atm}$. Solar oscillations will thus not fully develop in LBL experiments on Earth, but sub-leading effects play nevertheless an important role in precision experiments. Another modification comes from the fact that the neutrino beams of LBL experiments traverse the matter of the Earth. Coherent forward scattering in matter must therefore to be taken into account, which makes the analysis more involved, but it offers also unique opportunities.

The existing K2K experiment as well as MINOS and CNGS, which are both under construction, are a promising first generation of LBL experiments. We will discuss here (based on [9]) the remarkable potential beyond this first generation. One important point is that the increased precision will allow to test in detail the three-flavouredness of oscillations. We will also see that it will be possible to limit or measure θ_{13} drastically better than today. Next it will be possible to study in detail MSW matter effects and to extract in this way $\text{sign}(\Delta m_{31}^2)$, *i.e.* the mass ordering of the neutrino states. For the now favoured LMA solution it will be possible to mea-

*To appear in the proceedings of the XXth International Conference on Neutrino Physics and Astrophysics, "Neutrino 2002", Munich, Germany, May 25-30, 2002

sure leptonic CP violation [10]. The precise neutrino masses, mixings and CP phases which can be obtained in this way are extremely valuable information about flavour physics, since unlike for quarks these parameters are not obscured by hadronic uncertainties. These parameters can be evolved with the renormalization group *e.g.* to the GUT scale, where the rather precisely known parameters can be compared with mass models neutrino masses and mixings. Leptonic CP violation is moreover related to leptogenesis, the currently most plausible mechanism for the generation of the baryon asymmetry of the universe. LBL experiments offer therefore in a unique way access to precise knowledge on extremely interesting and valuable physics parameters.

2. Beams and Detectors

LBL experiments have the advantage that both source and detector can be kept under precise conditions. This includes amongst others for the source a precise knowledge of the mean neutrino energy E_ν , the neutrino flux and spectrum, as well as the flavour composition and contamination of the beam. Another important aspect is whether neutrino and anti-neutrino data can be obtained symmetrically such that systematical uncertainties cancel in an analysis. Precise measurements require also a sufficient luminosity and a detector such that enough statistics can be obtained. On the detector side one must include further issues, like the detection threshold function, energy calibration, resolution, particle identification capabilities (flavour, charge, event reconstruction, understanding backgrounds). Another source of uncertainty in the detection process is the knowledge of neutrino cross-sections, especially at low energies [11]. Source and detector combinations of a future LBL experiment are furthermore constraint by the available technology and one should keep potential improvements of source and detector developments in mind. An example is given by liquid argon detectors like ICARUS [12] which are not included in this study, but might become extremely valuable detectors or detector components in the future, improving the potential even further.

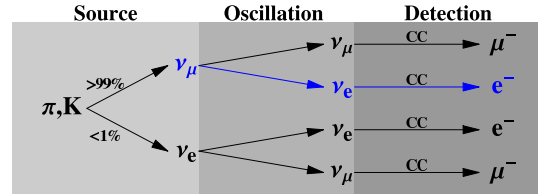


Figure 1. Neutrino production, oscillation and detection via charged current interactions for conventional beams and superbeams. Most interesting are the $\nu_\mu \rightarrow \nu_\mu$ disappearance and $\nu_\mu \rightarrow \nu_e$ appearance channels. The ν_e beam contamination at the level of $< 1\%$ limits the ability to determine the $\nu_\mu \rightarrow \nu_e$ appearance oscillation, since it produces also electrons. The ν_τ channel is not shown here, but it would become very important if tau lepton detection were feasible.

The first type of considered sources are conventional neutrino and anti-neutrino beams. An intense proton beam is typically directed onto a massive target producing mostly pions and some K mesons, which are captured by an optical system of magnets in order to obtain a beam. The pions (and K mesons) decay in a decay pipe, yielding essentially a muon neutrino beam which can undergo oscillations as shown in fig. 1. Most interesting are the $\nu_\mu \rightarrow \nu_\mu$ disappearance channel and the $\nu_\mu \rightarrow \nu_e$ appearance channels. The neutrino beam is, however, contaminated by approximately 0.5% electron neutrinos, which also produce electron reactions in the disappearance channel, limiting thus the precision in the extraction of $\nu_\mu \rightarrow \nu_e$ oscillation parameters. The energy spectrum of the muon beam can be controlled over a wide range: it depends on the incident proton energy, the optical system, and the precise direction of the beam axis compared to the direction of the detector. It is possible to produce broad band high energy beams, such as the CNGS beam [13,14], or narrow band lower energy beams, such as in some configurations of the NuMI beam [15]. Reversing the electrical current in the lens system results in an anti-neutrino

beam. The neutrino and anti-neutrino beams have significant differences such that errors do not cancel systematically in ratios or differences. The neutrino and anti-neutrino beams must therefore more or less be considered as independent sources with different systematical errors.

So-called “superbeams” are based on the same beam dump techniques for producing neutrino beams, but at much larger luminosities [13,14,15,16]. Superbeams are thus a technological extrapolation of conventional beams, but use a proton beam intensity close to the mechanical stability limit of the target at a typical thermal power of 0.7 MW to 4 MW. The much higher neutrino luminosity allows the use of the decay kinematics of pions to produce so-called “off-axis beams”, where the detector is located some degrees off the beam axis. This reduces the neutrino flux and the average neutrino energy, but leads to a more mono-energetic beam and a significant suppression of the electron neutrino contamination. Several off-axis superbeams with energies of about 1 GeV to 2 GeV have been proposed in Japan [17,18], America [19], and Europe [20,21].

The most sensitive neutrino oscillation channel for sub-leading oscillation parameters is the $\nu_\mu \rightarrow \nu_e$ appearance transition. Therefore the detector should have excellent electron and muon charged current identification capabilities. In addition, an efficient rejection of neutral current events is required, because the neutral current interaction mode is flavor blind. With low statistics, the magnitude of the contamination itself limits the sensitivity to the $\nu_\mu \rightarrow \nu_e$ transition severely, while the insufficient knowledge of its magnitude constrains the sensitivity for high statistics. A near detector allows a substantial reduction of the background uncertainties [17,22] and plays a crucial role in controlling other systematical errors, such as the flux normalization, the spectral shape of the beam, and the neutrino cross section at low energies. At energies of about 1 GeV, the dominant charge current interaction mode is quasi-elastic scattering, which suggests that water Cherenkov detectors are the optimal type of detector. At these energies, a baseline of about 300 km would be optimal to measure at the first maximum of the oscillation. At about

2 GeV, there is already a considerable contribution of inelastic scattering to the charged current interactions, which means that it would be useful to measure the energy of the hadronic part of the cross section. This favors low- Z hadron calorimeters, which also have a factor of ten better neutral current rejection capability compared to water Cherenkov detectors [19]. In this case, the optimum baseline is around 600 km. The matter effects are expected to be small for these experiments for two reasons. First of all, an energy of about 1 GeV to 2 GeV is small compared to the MSW resonance energy of approximately 13 GeV in the upper mantle of the Earth. The second reason is that the baseline is too short to produce significant matter effects.

The second type of beam considered are so-called neutrino factories, where muons are stored in the long straight sections of a storage ring. The decaying muons produce muon and electron anti-neutrinos in equal numbers [23]. The muons are produced by pion decays, where the pions are produced by the same technique as for superbeams. After being collected, they have to be cooled and reaccelerated very quickly. This has not yet been demonstrated and it is a major technological challenge. The spectrum and flavor content of the beam are completely characterized by the muon decay and are therefore very precisely known [24]. The only adjustable parameter is the muon energy E_μ , which is usually considered in the range from 20 to 50 GeV. In a neutrino factory it would be possible to produce and store anti-muons in order to obtain a CP conjugated beam. The symmetric operation of both beams leads to the cancellation or significant reduction of errors and systematical uncertainties. We will discuss in the following the neutrino beam, which implies always implicitly – unless otherwise stated – the CP conjugate channel.

The decay of the muons and the relevant oscillation channels are shown in fig. 2. Amongst all flavors and interaction types, muon charged current events are the easiest to detect. The appearance channel with the best sensitivity is thus the $\bar{\nu}_e \rightarrow \bar{\nu}_\mu$ transition, which produces so called “wrong sign muons”. Therefore, a detector must be able to very reliably identify the charge of a

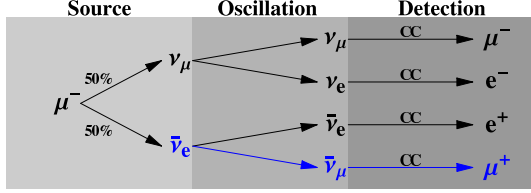


Figure 2. Neutrino production, oscillation and detection via charged current interactions for a neutrino factory for one polarity. $\bar{\nu}_e$ and ν_μ are produced in equal numbers from μ -decays and can undergo different oscillations. The $\nu_\mu \rightarrow \nu_\mu$ and $\bar{\nu}_e \rightarrow \bar{\nu}_\mu$ channels are most interesting for detectors with μ identification. Note, however, that excellent charge identification capabilities are required to separate “wrong sign muons” and “right sign muons”. The ν_τ oscillation channel is not shown here, but it would become important for detectors with tau identification capabilities.

muon in order to distinguish wrong sign muons in the appearance channel from the higher rate of same sign muons in the disappearance channels. The dominant charge current interaction in the multi-GeV range is deep-inelastic scattering, making a good energy resolution for the hadronic energy deposition necessary. Magnetized iron calorimeters are thus the favored choice for neutrino factory detectors. In order to achieve the required muon charge separation, it is necessary to impose a minimum muon energy cut at approximately 4 GeV [25,26]. This leads to a significant loss of neutrino events in the range of about 4 GeV to 20 GeV, which means that a high muon energy of $E_\mu = 50$ GeV is desirable. The first oscillation maximum lies then at approximately 3000 km. Matter effects are sizable at this baseline and energy, and the limited knowledge of the Earth’s matter density profile becomes an additional source of errors.

3. The Oscillation Framework

The general three neutrino oscillation probabilities in matter are quite lengthy expressions. It is useful to simplify them such that an analytic understanding becomes possible. Quantitative results should, however, be obtained in numerical calculations using the full expressions. The key to an analytic simplification is to expand the oscillation probabilities in small quantities, namely $\alpha = \Delta m_{21}^2 / \Delta m_{31}^2 \simeq 10^{-2}$ and $\sin^2 2\theta_{13} \leq 0.1$. The matter effects can be parametrized by the dimensionless quantity $\hat{A} = A / \Delta m_{31}^2 = 2VE / \Delta m_{31}^2$, where $V = \sqrt{2}G_F n_e$. Using $\Delta \equiv \Delta_{31}$, the leading terms in this expansion are [27,28,29]

$$P(\nu_\mu \rightarrow \nu_\mu) \approx 1 - c_{13}^2 s_{23}^2 \sin^2 \Delta + 2\alpha c_{13}^2 c_{12}^2 s_{23}^2 \Delta \cos \Delta \quad (1)$$

$$\begin{aligned} P(\nu_e \rightarrow \nu_\mu) \approx & s_{13}^2 s_{23}^2 \frac{\sin^2((1-\hat{A})\Delta)}{(1-\hat{A})^2} \\ & \pm s_\delta \hat{s}_{13} \alpha \hat{s}_{12} c_{13} \hat{s}_{23} \sin(\Delta) \frac{\sin(\hat{A}\Delta) \sin((1-\hat{A})\Delta)}{\hat{A}(1-\hat{A})} \\ & + c_\delta \hat{s}_{13} \alpha \hat{s}_{12} c_{13} \hat{s}_{23} \cos(\Delta) \frac{\sin(\hat{A}\Delta) \sin((1-\hat{A})\Delta)}{\hat{A}(1-\hat{A})} \\ & + \alpha^2 \hat{s}_{12}^2 c_{23}^2 \frac{\sin^2(\hat{A}\Delta)}{\hat{A}^2} \end{aligned} \quad (2)$$

where $s_{ij} = \sin \theta_{ij}$, $c_{ij} = \cos \theta_{ij}$, $\hat{s}_{ij} = \sin 2\theta_{ij}$, $\hat{c}_{ij} = \cos 2\theta_{ij}$, $s_\delta = \sin \delta$, $c_\delta = \cos \delta$, and where in eq. (2) “+” stands for neutrinos and “−” for anti-neutrinos. The most important feature of eq. (2) is that all interesting effects in the $\nu_e \rightarrow \nu_\mu$ transition depend crucially on θ_{13} . The size of $\sin^2 2\theta_{13}$ determines thus if the total transition rate, matter effects, effects due to the sign of Δm_{31}^2 and CP violating effects are measurable. One of the most important questions for future LBL experiments is therefore how far experiments can push the θ_{13} limit below the current CHOOZ bound of approximately $\sin^2 2\theta_{13} < 0.1$.

Before we discuss further important features of eqs. (1) and (2) in more detail we would like to comment once more on the underlying assumptions and the reliability of these equations. First eqs. (1) and (2) are an expansion in terms of the small quantities α and $\sin 2\theta_{13}$. Higher order terms are suppressed at least by another power of one of these small parameters and these corrections are thus typically at the percent level.

The matter corrections in eqs. (1) and (2) are derived for constant average matter density. Numerical tests have shown that this approximation works quite well as long as the matter profile is reasonably smooth. A number of very interesting effects existing in general non-constant matter distributions are therefore only small theoretical uncertainties. An example is given by asymmetric matter profiles, which lead to interesting T-violating effects [30], but this does not play a role here since the Earth is sufficiently symmetric.

Note that all results which will be shown later are based on numerical simulations of the full problem in matter. These results do therefore not depend on any approximation. Eqs. (1) and (2) will only be used to understand the problem analytically, which is extremely helpful in order to oversee the six (or more) dimensional parameter space. The full numerical analysis and eqs. (1) and (2) depend, however, on the assumption of a standard three neutrino scenario. It is thus assumed that the LSND signal [31] will not be confirmed by the MiniBooNE experiment [32]. Neutrinos could in principle decay, which would make the analysis much more involved. It is assumed in this article that neutrinos are stable, and a combined treatment of oscillation and decay [33] would be much more involved. Neutrinos might further have unusual properties and might, for example, violate CPT. In that case neutrinos and anti-neutrinos could have different properties and LBL experiments can give very interesting limits on this possibility [34], but we will assume in this study that CPT is preserved.

4. Correlations and Degeneracies

Eqs. (1) and (2) exhibit certain parameter correlations and degeneracies, which play an important role in the analysis of LBL experiments, and which would be hard to understand in a purely numerical analysis of the high dimensional parameter space. The most important properties are:

- First we observe that eqs. (1) and (2) depend only on the product $\alpha \cdot \sin 2\theta_{12}$ or equivalently $\Delta m_{21}^2 \cdot \sin 2\theta_{12}$. This are the parameters related to solar oscillations which will be taken as external input. The

fact that only the product enters, implies that it may be better determined than the product of the measurements of Δm_{21}^2 and $\sin 2\theta_{12}$.

- Next we observe in eq. (2) that the second and third term contain both a factor $\sin(\hat{A}\Delta)$, while the last term contains a factor $\sin^2(\hat{A}\Delta)$. Since $\hat{A}\Delta = 2VL$, we find that these factors depend only on L , resulting in a “magic baseline” when $2VL_{magic} = \pi/4V$, where $\sin(\hat{A}\Delta)$ vanishes. At this magic baseline only the first term in eq. (2) survives and $P(\nu_e \rightarrow \nu_\mu)$ does no longer depend on δ , α and $\sin 2\theta_{12}$. This is in principle very important, since it implies that $\sin^2 2\theta_{13}$ can be determined at the magic baseline from the first term of eq. (2) whatever the values and errors of δ , α and $\sin 2\theta_{12}$ are. For the matter density of the Earth we find

$$L_{magic} = \pi/4V \simeq 8100 \text{ km} , \quad (3)$$

which is an amazing number, since the value of V could be such that L_{magic} is very different from the scales under discussion.

- Next we observe that only the second and third term of eq. (2) depend on the CP phase δ , and both terms contain a factor $\sin 2\theta_{13} \cdot \alpha$, while the first and fourth term of eq. (2) do not depend on the CP phase δ and contain factors of $\sin^2 2\theta_{13}$ and α^2 , respectively. The extraction of CP violation is thus always suppressed by the product $\sin 2\theta_{13} \cdot \alpha$ and the CP violating terms are furthermore obscured by large CP independent terms if either $\sin^2 2\theta_{13} \ll \alpha^2$ or $\sin^2 2\theta_{13} \gg \alpha^2$. The determination of the CP phase δ is thus best possible if $\sin^2 2\theta_{13} \simeq 4\theta_{13}^2 \simeq \alpha^2$.
- The last term in eq. (2), which is proportional to $\alpha^2 = (\Delta m_{21}^2)^2/(\Delta m_{31}^2)^2$, dominates for tiny $\sin^2 2\theta_{13}$. The error of Δm_{21}^2 limits therefore for small $\sin^2 2\theta_{13}$ the parameter extraction.

- Eqs. (1) and (2) suggest the existence of degeneracies, *i.e.* for given L/E parameter sets with identical oscillation probabilities. An example is given by a simultaneous replacement of neutrinos by anti-neutrinos and $\Delta m_{31}^2 \rightarrow -\Delta m_{31}^2$. This is equivalent to changing the sign of the second term of eq. (2) and replacing $\alpha \rightarrow -\alpha$ and $\Delta \rightarrow -\Delta$, while $\hat{A} \rightarrow \hat{A}$. Eqs. (1) and (2) are unchanged, but this does not constitute a degeneracy, since neutrinos and anti-neutrinos can be distinguished experimentally.
- The first real degeneracy [35] can be seen in the disappearance probability eq. (1), which is invariant under $\theta_{23} \rightarrow \pi/2 - \theta_{23}$. Note that the second and third term in eq. (2) are not invariant under this transformation, but this change in the sub-leading appearance probability can approximately be compensated by small parameter shifts. However, the degeneracy can in principle be lifted with precision measurements in the disappearance channels.
- The second degeneracy can be found in the appearance probability eq. (2) in the $(\delta - \theta_{13})$ -plane [36]. In terms of θ_{13} (which is small) and δ the four terms of eq. (2) have the structure

$$P(\nu_e \rightarrow \nu_\mu) \approx \theta_{13}^2 \cdot F_1 + \theta_{13} \cdot (\pm \sin \delta F_2 + \cos \delta F_3) + F_4 \quad (4)$$

where the quantities F_i , $i = 1, \dots, 4$ contain all the other parameters. The requirement $P(\nu_e \rightarrow \nu_\mu) = \text{const.}$ leads for both neutrinos and anti-neutrinos to parameter manifolds of degenerate or correlated solutions. Having both neutrino and anti-neutrino beams, the two channels can be used independently, which is equivalent to considering simultaneously eq. (4) for $F_2 \equiv 0$ and $F_3 \equiv 0$. The requirement that these probabilities are now independently constant, *i.e.* $P(\nu_e \rightarrow \nu_\mu) = \text{const.}$ for $F_2 \equiv 0$ and $F_3 \equiv 0$, leads to more constraint manifolds in the $(\delta - \theta_{13})$ -plane, but some degeneracies still survive.

- The third degeneracy [37] is given by the fact that a change in sign of Δm_{31}^2 can essentially be compensated by an offset in δ . Therefore we note again that the transformation $\Delta m_{31}^2 \rightarrow -\Delta m_{31}^2$ leads to $\alpha \rightarrow -\alpha$, $\Delta \rightarrow -\Delta$ and $\hat{A} \rightarrow -\hat{A}$. All terms of the disappearance probability, eq. (1), are invariant under this transformation. The first and fourth term in the appearance probability eq. (1), which do not depend on the CP phase δ , are also invariant. The second and third term of eq. (1) depend on the CP phase and change by the transformation $\Delta m_{31}^2 \rightarrow -\Delta m_{31}^2$. The fact that these changes can be compensated by an offset in the CP phase δ is the third degeneracy.
- Altogether there exists an eight-fold degeneracy [35], as long as only the $\nu_\mu \rightarrow \nu_\mu$, $\bar{\nu}_\mu \rightarrow \bar{\nu}_\mu$, $\nu_e \rightarrow \nu_\mu$ and $\bar{\nu}_e \rightarrow \bar{\nu}_\mu$ channels and one fixed L/E are considered. However, the structure of eqs. (1) and (2) makes clear that the degeneracies can be broken by using in a suitable way information from different L/E values. This can be achieved in total event rates by changing L or E [38,39], but it can in principle also be done by using information in the event rate spectrum of a single baseline L , which requires detectors with very good energy resolution [29]. Another way to break the degeneracies is to include further oscillation channels in the analysis (“silver channels”) [40,38].

The discussion shows the strength of the analytic approximations, which allow to understand the complicated parameter interdependence. It also helps to optimally plan experimental setups and to find strategies to resolve the degeneracies.

5. Event Rates

The experimentally observed events must be compared with the theoretical expressions, which depend only indirectly on the above oscillation probabilities [9]. Every event can be classified by the information on the flavor of the detected neutrino and the type of interaction. The particles detected in an experiment are produced by

neutral current (NC), inelastic charged current (CC) or quasi-elastic charged current (QE) interactions. The contribution to each mode depends on a number of factors, like detector type, the neutrino energy and flavour. To determine realistic event rates we compute first for each neutrino flavor and energy bin the number of events for each type of interaction in the fiducial mass of an ideal detector. Next the deficiencies of a real detector are included, like limited event reconstruction capabilities. The combined description leads to the differential event rate spectrum for each flavor and interaction mode as it would be seen by a detector which is able to separate all these channels. Finally different channels must be combined, if they can not be observed separately. This can be due to physics, *e.g.*, due to the flavor-blindness of NC interactions, or it can be a consequence of detector properties, *e.g.*, due to charge misidentification. In order to include backgrounds, the channels are grouped in an experiment specific way into pairs of signal and background. The considered backgrounds are NC-events which are misidentified as CC-events and CC-events identified with the wrong flavor or charge. For superbeams the background of CC-events coming from an intrinsic contamination of the beam is included. Finally all available signal channels are combined in a global analysis in order to optimally extract the physics parameters. The relevant channels are for a neutrino factory for each polarity of the beam the ν_μ -CC channel (disappearance) and $\bar{\nu}_\mu$ -CC channel (appearance) event rate spectra. The backgrounds for these signals are NC events for all flavours and misidentified ν_μ -CC events. For superbeam experiments the signal is for each polarity of the beam given by the ν_μ -QE channel (disappearance) and ν_e -CC channel (appearance). The backgrounds are here NC events for all flavors, misidentified ν_μ -CC events, and, for the ν_e -CC channel, the ν_e -CC beam contamination.

6. The Considered LBL Setups

The discussed sources and detectors allow different LBL experiments and it is interesting to compare their physics potential on an equal and

as realistic as possible footing. Studies at the level of probabilities are not sufficient and the true potential must be evaluated at the level of event rates as described in section 5, with realistic assumptions about the beams, detectors and backgrounds. We present now the results of such an analysis which is essentially based on reference [9], where we calculate the oscillation probabilities with the exact three neutrino oscillation formulae in matter numerically, *i.e.* we use the approximations for the probabilities in eqs. (1) and (2) only for a qualitative understanding. All results shown below are therefore not affected by approximations which were made in the derivation of the approximate analytic oscillation formulae eqs. (1) and (2). Sensitivities etc. are defined by the ability to re-extract the physics parameters from a simulation of event rates. Therefore event rate distributions are generated for any possible parameter set. Subsequently a combined fit to these event rate distributions is performed simultaneously for the appearance and disappearance channels for both polarities. This procedure uses all the available information in an optimal way. It includes spectral distributions when present, and it reduces to a fit of total rates when the total event rates are small. Adequate statistical methods as described in [9] are used in order to deal with event distributions which have in some regions small event rates per bin. Systematical uncertainties are parametrized and external input from geophysics is used in form of the detailed matter profile and its errors, which are included in the analysis [9]. The ability to re-extract in a simulation of the full experiment the input parameters which were used to generate event rate distributions is used to define sensitivities and precision.

It is important to include in the analysis external information. The discussed LBL experiments could in principle measure the solar Δm_{21}^2 and mixing angle θ_{12} . However, the precision which can be obtained can not compete with the expected measurement of KamLand [41]. We include therefore as external input the assumption that KamLand measures the solar parameters in the center of the LMA region with typical errors. Otherwise all unknown parameters (like the CP

phase) will not be constrained and are therefore left free, with all parameter degeneracies and error correlations taken into account. All nuisance parameters are integrated out and a projection on the parameter of interest is performed. Altogether we are dealing with six free parameters.

We include the beam characteristics of the three considered sources as well as uncertainties of these beam parameters, *i.e.* for the conventional JHF and NuMI off-axis beams uncertainties in the ν_e -background and for all beams flux uncertainties [17,19,23]. As detectors we consider water Cherenkov detectors, low-Z calorimeters and magnetized iron detectors. For magnetized iron calorimeters it is important to include realistic threshold effects. We use a linear rise of the efficiency between 4 GeV and 20 GeV and we study the sensitivity to the threshold position. We do not include liquid Argon TPCs in our analysis, but they would certainly be an important detector if this technology will work. The considered beams and detectors allow now different interesting combinations which are listed in table 1. JHF-SK is the planned combination of the existing SuperKamiokande detector and the JHF beam, while JHF-HK is the combination of an upgraded JHF beam with the proposed Hyper-Kamiokande detector. With typical parameters, JHF-HK is altogether about 95 times more integrated luminosity than JHF-SK, and we assume that it operates partly with the anti-neutrino beam. Water Cherenkov detectors are ideal for the JHF beam, since charged current quasi elastic scattering is dominating. A low-Z calorimeter is proposed for the NuMI off-axis beam, which is better here, since the energy is higher and there is already a considerable contribution of inelastic charged current interactions. NuFact-I is an initial neutrino factory, while NuFact-II is a fully developed machine, with 42 times the luminosity of NuFact-I [17,19,25]. Deep inelastic scattering dominates for these even higher energies and magnetized iron detectors are therefore considered in combination with neutrino factories.

acronym	detector	L	L/E_{peak}
JHF-SK	water Cherenkov	295	378
NuMI	low-Z	735	337
NuFact-I	10 kt mag. iron	3000	90
JHF-HK	water Cherenkov	735	295
NuFact-II	40 kt mag. iron	3000	90

Table 1

The considered combinations of beams and detectors and their acronyms.

7. Results

A realistic analysis of future LBL experiments requires a number of different aspects to be taken into account. It should be clear from the discussion above that it is not sufficient to quote limits which are based on oscillation probabilities or merely on the statistics of a single channel without backgrounds or systematics. Depending on the position in the space of physics parameters the degeneracies or correlations, the backgrounds, the systematics or statistics may be the limiting factor. A reliable comparative study of the discussed LBL setups requires therefore a detailed analysis of the six dimensional parameter space, which includes all these effects on the same footing [9].

There is excellent precision for the leading oscillation parameters Δm_{31}^2 and $\sin^2 2\theta_{23}$, which will not be further discussed here. The more interesting sensitivity to the sub-leading parameter $\sin^2 2\theta_{13}$ depends on what will be found for Δm_{31}^2 and Δm_{21}^2 . Assuming that the leading parameters are measured to be $\Delta m_{31}^2 = 3 \cdot 10^{-3} \text{ eV}^2$, $\sin^2 2\theta_{23} = 0.8$ and that KamLand measures the solar parameters at the current best fit point of the LMA region, *i.e.* $\Delta m_{21}^2 = 6 \cdot 10^{-5} \text{ eV}^2$ and $\sin 2\theta_{12} = 0.91$, we can make a comparison of the $\sin^2 2\theta_{13}$ sensitivity limit for the different setups. The result is shown in fig. 3. The individual contributions of different sources of uncertainties are shown for every experiment and the left edge of every band in fig. 3 corresponds to the sensitivity limit which would be obtained purely on statistical grounds. This limit is successively reduced by

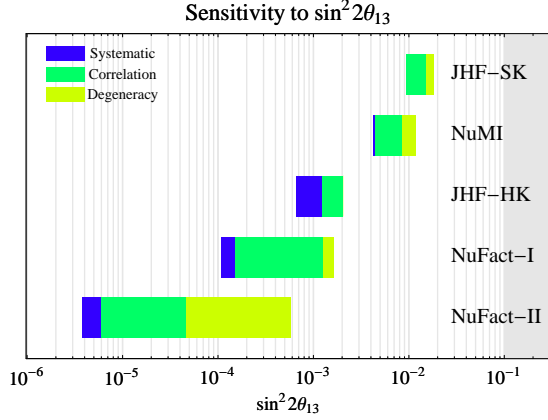


Figure 3. The $\sin^2 2\theta_{13}$ sensitivity for all setups defined in section 6 at the 90% confidence level for $\Delta m_{31}^2 = 3 \cdot 10^{-3} \text{ eV}^2$ and $\sin^2 2\theta_{23} = 0.8$. The plot shows the deterioration of the sensitivity limits as the different error sources are successively switched on. The left edge of the bars is the sensitivity statistical limit. This limit gets reduced as systematic, correlational and degeneracy errors are switched on. The right edge is the final sensitivity limit [9].

adding the systematical uncertainties of each experiment, the correlational errors and finally the degeneracy errors. The right edge of each band constitutes the final error for the experiment under consideration. It is interesting to see how the errors of the different setups are composed. There are different sensitivity reductions due to systematic errors, correlations and degeneracies. The largest sensitivity loss due to correlations and degeneracies occurs for NuFact-II, which is mostly a consequence of the uncertainty of Δm_{21}^2 , which translates into an α uncertainty, and which dominates the appearance probability eq. (2) for small $\sin^2 2\theta_{13}$. Note that it is in principle possible to combine different experiments. If done correctly, this allows to eliminate part or all of the correlational and degeneracy errors [38].

Another challenge of future LBL experiments is to measure $\text{sign}(\Delta m_{31}^2)$ via matter effects and

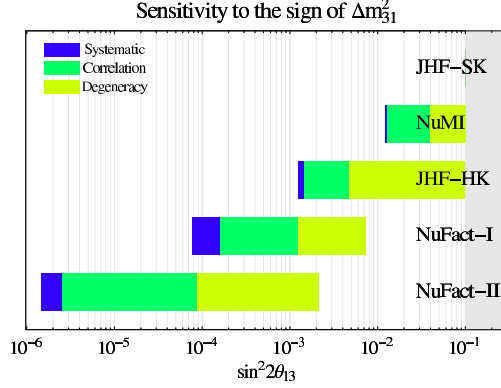


Figure 4. The $\sin^2 2\theta_{13}$ sensitivity region to $\text{sign}(\Delta m_{31}^2)$ for the setups defined in section 6. The left edge of the bars are the statistical sensitivity limits which are successively reduced by systematical, correlational and degeneracy errors. The right edge of the bars is the final limit.

the sensitivity which can be obtained for the setups under discussion is shown in fig. 4. Taking all correlational and degeneracy errors into account we can see that it is very hard to determine $\text{sign}(\Delta m_{31}^2)$ with the considered superbeam setups. The main problem is the degeneracy with δ , which allows always the reversed $\text{sign}(\Delta m_{31}^2)$ for another CP phase. Note, however, that the situation can in principle be improved if different superbeam experiments were combined such that this degeneracy error could be removed. Neutrino factories perform considerably better on $\text{sign}(\Delta m_{31}^2)$, particularly for larger baselines. Combination strategies would again lead to further improvements.

Coherent forward scattering of neutrinos and the corresponding MSW matter effects are so far experimentally untested. It is therefore very important to realize that matter effects will not only be useful to extract $\text{sign}(\Delta m_{31}^2)$, but that they allow also detailed tests of coherent forward scattering of neutrinos. This has been studied in detail in [29,42,43,44].

The Holy Grail of LBL experiments is the mea-

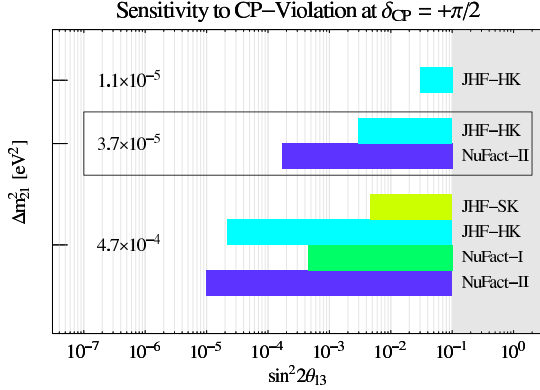


Figure 5. The $\sin^2 2\theta_{13}$ sensitivity range for CP violation of the considered setups at 90% confidence level and for different Δm^2_{21} values. The upper row corresponds to the lower bound of $\Delta m^2_{21} = 1.1 \times 10^{-5} \text{ eV}^2$, the bottom row to the upper bound $\Delta m^2_{21} = 4.7 \times 10^{-4} \text{ eV}^2$, and the middle row to the best LMA fit, $\Delta m^2_{21} = 3.7 \times 10^{-5} \text{ eV}^2$. Cases which do not have CP sensitivity are omitted from this plot. The chosen parameters are $\delta = +\pi/2$, $\Delta m^2_{31} = 3 \cdot 10^{-3} \text{ eV}^2$, $\sin^2 2\theta_{23} = 0.8$, and a solar mixing angle corresponding to the current best fit in the LMA regime [9].

surement of leptonic CP violation. The $\sin^2 2\theta_{13}$ sensitivity range for measurable CP violation is shown in fig. 5 for $\delta = \pi/2$ for the different setups and for different values of Δm^2_{21} . It can be seen that measurements of CP violation are in principle feasible both with high luminosity superbeams as well as advanced neutrino factories. However, the sensitivity depends in a crucial way on Δm^2_{21} . For a low value $\Delta m^2_{21} = 1.1 \cdot 10^{-5} \text{ eV}^2$, the sensitivity is almost completely lost, while the situation would be very promising for the largest considered value $\Delta m^2_{21} = 4.7 \cdot 10^{-4} \text{ eV}^2$. For a measurement of leptonic CP violation it would therefore be extremely exciting and promising if KamLand would find Δm^2_{21} on the high side of the LMA solution (the so-called HLMA case). The sensitivities shown in fig. 5 depend on the

choice for δ . The value which was used here was $\delta = \pi/2$ and the sensitivities become worse for small CP phases close to zero or π .

8. Conclusions

Future long baseline neutrino oscillation experiments will lead to precision neutrino physics. A basic fact which makes this possible is that the atmospheric mass splitting $\Delta m^2_{31} \simeq \Delta m^2_{\text{atm}}$ leads for typical neutrino energies $E_\nu \simeq 1 - 100 \text{ GeV}$ to oscillation baselines in the range 100 km to 10000 km. Beams have the advantage, that unlike the sun or the atmosphere, they can be controlled very precisely. Combined with equally precise detectors and an adequate oscillation framework (including three neutrinos and matter effects) must be used. There exist different interesting sources for long baseline oscillation experiments, like reactors or β -beams, but we restricted the discussion here to superbeams and neutrino factories. We presented the issues which enter into realistic assessments of the potential of such experiments. The discussed experiments turned out to be very promising and they lead to very precise measurements of the leading oscillation parameters Δm^2_{31} and $\sin^2 2\theta_{23}$. We discussed in detail how the different setups lead to very interesting measurements or limits θ_{13} and δ . It will also be possible to perform impressive tests of Earth matter effects, allowing to extract $\text{sign}(\Delta m^2_{31})$. The discussed setups have an increasing potential and increasing technological challenges, but it seems possible to build them in stages. The shown results are valid for each individual setup and future results should of course be included in the analysis. This would be especially important if more LBL experiments were built and depending on previous results there exist different optimization strategies. In the short run the expected results from KamLand are extremely important and will have considerable impact. First it will become clear if Δm^2_{21} lies in the LMA regime, which is very important since realistically, CP violation can only be measured then. Within the LMA solution it is also very important if Δm^2_{21} lies close to the current best fit, on the high or on the low side. A value of Δm^2_{21} on the high side

(HLMA) would be ideal, since it would guarantee an extremely promising LBL program with a chance to see leptonic CP violation already with the JHF beam in the next decade.

REFERENCES

1. T. Toshito (SuperKamiokande Collab.), [hep-ex/0105023](#).
2. Q. R. Ahmad *et al.* (SNO Collab.), Phys. Rev. Lett. **89**, 011301 (2002).
3. Q. R. Ahmad *et al.* (SNO Collab.), Phys. Rev. Lett. **89**, 011302 (2002).
4. V. Barger, D. Marfatia, K. Whisnant and B. P. Wood, Phys. Lett. **B537**, 179 (2002).
5. A. Bandyopadhyay, S. Choubey, S. Goswami and D. P. Roy, [hep-ph/0204286](#).
6. J. N. Bahcall, M. C. Gonzalez-Garcia and C. Peña-Garay, [hep-ph/0204314](#).
7. P. C. de Holanda and A. Yu. Smirnov, [hep-ph/0205241](#).
8. M. Apollonio *et al.* (Chooz Collab.), Phys. Lett. **B466**, 415 (1999).
9. P. Huber, M. Lindner and W. Winter, [hep-ph/0204352](#).
10. K. Dick, M. Freund, M. Lindner and A. Romanino, Nucl. Phys. B **562** (1999) 29.
11. E.A. Paschos, [hep-ph/0204138](#).
12. F. Arneodo *et al.*, (ICARUS Collab.), Nucl. Instr. Meth. A **471**, 272 (2000).
13. G. Acquistapace *et al.* (CNGS Collab.) CERN-98-02.
14. R. Baldy *et al.* (CNGS Collab.) CERN-SL-99-034-DI.
15. J. Hylen *et al.* (NuMI Collab.) FERMILAB-TM-2018.
16. K. Nakamura (K2K Collab.), Nucl. Phys. **A663**, 795 (2000).
17. Y. Itow *et al.*, [hep-ex/0106019](#).
18. M. Aoki, [hep-ph/0204008](#).
19. A. Para and M. Szleper, [hep-ex/0110032](#).
20. See e.g. J.J. Gomez-Cadenas *et al.*, [hep-ph/0105297](#).
21. F. Dydak, Tech.Rep., CERN (2002), <http://home.cern.ch/dydak/oscexp.ps>.
22. M. Szleper and A. Para, [hep-ex/0110001](#).
23. S. Geer, Phys. Rev. **D57**, 6989 (1998).
24. Particle Data Group, D.E. Groom *et al.*, Eur.Phys.J. C **15**, 1 (2000).
25. A. Blondel *et al.*, Nucl. Instrum. Meth. **A451**, 102 (2000).
26. C. Albright *et al.*, [hep-ex/0008064](#), and references therein.
27. A. Cervera *et al.*, Nucl. Phys. **B579**, 17 (2000), err. ibid., Nucl. Phys. **B593**, 731(2001).
28. M. Freund, Phys. Rev. **D64**, 053003 (2001).
29. M. Freund, P. Huber, and M. Lindner, Nucl. Phys. **B615**, 331 (2001).
30. E. Akhmedov, P. Huber, M. Lindner and T. Ohlsson, Nucl.Phys. B608 (2001) 394.
31. E.D. Church, K. Eitel, G.B. Mills and M. Steidl, Phys. Rev. D **66**, 013001 (2002).
32. E.A. Hawker, Int. J. Mod. Phys. A **16S1B**, 755 (2001).
33. M. Lindner, T. Ohlsson and W. Winter, Nucl. Phys. B 607 (2001) 326.
34. S.M. Bilenky, M. Freund, M. Lindner, T. Ohlsson and W. Winter, Phys. Rev. D **65** (2002) 073024.
35. V. Barger, D. Marfatia, and K. Whisnant, Phys. Rev. **D65**, 073023 (2002).
36. J. Burguet-Castell, M.B. Gavela, J.J. Gomez-Cadenas, P. Hernandez and O. Mena, Nucl. Phys. **B608**, 301 (2001).
37. H. Minakata and H. Nunokawa, JHEP **10**, 001 (2001).
38. J. Burguet-Castell, M.B. Gavela, J.J. Gomez-Cadenas, P. Hernandez and O. Mena, [hep-ph/0207080](#).
39. V. Barger, D. Marfatia and K. Whisnant, [hep-ph/0206038](#).
40. A. Donini, D. Meloni and P. Migliozzi, [hep-ph/0206034](#).
41. V. Barger, D. Marfatia, and B. Wood, Phys. Lett. **B498**, 53 (2001).
42. M. Freund, M. Lindner, S. T. Petcov and A. Romanino, Nucl. Phys. **B578**, 27 (2000).
43. M. Freund, P. Huber, and M. Lindner, Nucl. Phys. **B585**, 105 (2000).
44. M. Freund, M. Lindner, S.T. Petcov and A. Romanino, Nucl. Instrum. Meth. A **451**, 18 (2000).